11-1-1992

Identification of the ns and nd Rydberg states of O2 for n=3–5

Robert J. Yokelson
University of Montana - Missoula, bob.yokelson@umontana.edu

R. J. Lipert
USDOE Ames Laboratory

W. A. Chupka
Yale University

Identification of the ns and nd Rydberg states of O2 for n=3–5

R. J. Yokelson, R. J. Lipert, and W. A. Chupka

Citation: The Journal of Chemical Physics **97**, 6153 (1992); doi: 10.1063/1.463724
View online: http://dx.doi.org/10.1063/1.463724
View Table of Contents: http://scitation.aip.org/content/aip/journal/jcp/97/9?ver=pdfcov
Published by the AIP Publishing

Identification of the $ns\sigma$ and $nd\lambda$ Rydberg states of O_2 for $n=3$–5

R. J. Yokelson,[a] R. J. Lipert,[b] and W. A. Chupka
Yale University Department of Chemistry, 225 Prospect St., New Haven, Connecticutt 06511

(Received 23 September 1991; accepted 28 October 1991)

The 4*s*–3*d* and 5*s*–4*d* Rydberg complexes of diatomic oxygen have been studied by (2 + 1) resonance-enhanced multiphoton ionization of the $X\,^3\Sigma_g^-$ ground state of O_2. We have located and identified at least two vibrational levels of each of the following states: Three of four expected $4s\sigma\ \Pi$ states; all four expected $5s\sigma\ \Pi$ states; 18 of 22 expected 3*d* states (with only the states of the $3d\sigma$ orbital remaining unobserved); and 5 of the 10 predicted $4d\pi$ states. State assignments were assisted by the following: the results of rotational cooling and laser polarization experiments which facilitated the rotational analysis, band positions, band intensities, and parameterized calculations. The experimentally determined state locations are compared with the state locations obtained from *ab initio* calculations. We have carried out isotope experiments and rotational linewidth analysis to study in some detail the mixing between the Rydberg states and the repulsive valence states as well as the mixing between the Rydberg states themselves. We conclude that direct predissociation dominates indirect predissociation as a dissociative mechanism, but there is evidence of $\Delta v \neq 0$ interactions which perturb the rotational structure of the $3d\pi\ \Sigma$ and Δ states. The relative intensities of the states detected are found to span a range in excess of 10^4 with the $ns\sigma\ \Pi$ states being the weakest and the $nd\pi\ \Sigma$ states being the strongest. Photoionization of the $nd\pi\ \Sigma$ states appears to be most affected by the shape resonance in the continuum. Our measurements confirm the expectation that many of the properties of the Rydberg states in the same series scale as $(n^*)^{-3}$.

I. INTRODUCTION

In earlier studies of O_2 by two-photon resonant photoionization spectroscopy the $3d\ ^{1,3}\Delta$ and $^{1,3}\phi$ Rydberg states converging to the ground state of the ion were identified and characterized as were some Σ states as well.[1] However, in those studies, carried out with moderate laser powers, some Σ states remained either undetected or only poorly characterized and no Π states were detected at all, including *ns* states with $n > 3$. The inability to detect Π states was ascribed as due to strong predissociation of the resonant state leading to low photoionization probability.

In the present study, the same spectral region was studied with a more powerful laser, improved detection sensitivity, and more accurate wavelength calibration, leading to the detection and assignment of all *ns* and *nd* ($n \leqslant 5$) Rydberg states except those Π states with the $nd\sigma$ configuration.

II. EXPERIMENTAL

The frequency doubled output of a XeCl excimer pumped, pulsed dye laser was polarization selected and then focused into a molecular beam inside a time-of-flight mass spectrometer. O_2^+ and O^+ ions created by the 2 + 1 REMPI process occurring in the beam were detected by triple microchannel plates. This signal was amplified and stored as a function of laser wavelength in an LSI-11 computer. For many scans the simultaneously observed optogalvanic signal due to atomic uranium and neon or argon was stored in a separate companion file. The dye laser was stepped in increments of 0.001 nm with the results of 50 to 150 laser shots being signal averaged at each increment. In the wavelength region used, 481.1 to 430 nm, the bandwidth of the dye laser fundamental was measured to be between 0.15 to 0.2 cm^{-1}, which corresponds to three to four wavelength increments. In all, some 300 wavelength scans were performed to determine the absolute transition energies and to probe the effects of laser power, laser polarization, rotational temperature, and isotopic substitution on various parts of the spectrum.

The main source of error in measuring the absolute energies is undesired nonlinearity in the laser wavelength tuning system. For nearly all scans this led to a worst case error of less than 0.5 cm^{-1} for the state energy. Laser power (for the doubled light) varied from 0.1 to 1 mj/pulse. The higher powers caused some broadening of the peaks but were necessary to detect the strongly homogeneously predissociated Π states. (For these states the signal intensity was proportional to the third power of the doubled light.) The laser polarization experiments used a double and single rhomb and enabled us to locate the *Q* lines of Σ states as explained in Ref. 1.

The molecular rotational temperature was varied by the use of various types of cw and pulsed nozzles and also by varying gas mixture, backing pressure, location of ionization in the molecular beam, and, for the pulsed nozzles, timing with respect to the laser triggering pulse and driver pulse

[a] Present address: Cooperative Institute for Research in Environmental Sciences, University of Colorado/NOAA, Boulder, CO 80309-0216.
[b] Present address: Ames Laboratory USDOE, Iowa State University, Ames, Iowa 50011.

width. Several rotational temperatures were useful in the analysis. The best cooling (≈ 1 K) resulted in spectra with $>90\%$ of the intensity due to transitions from the $N'' = 1$ levels of O_2. Such data served to locate the band origins. Slightly warmer (≈ 10 K) spectra gave more lines to enhance the reliability of the rotational analysis. The isotope experiments were undertaken primarily to change the energy gap between states thought to mix by $\Delta v \neq 0$ interactions.

III. RESULTS AND DISCUSSION

A. General

Ab initio calculations, described in Ref. 2, were performed by Lefebvre-Brion to predict the location of the $v' = 0$ level of all 22 $3d\lambda$ Rydberg states. As an aid to discussing the present data the results of these calculations are shown in Fig. 1 and they are compared with the experimen-

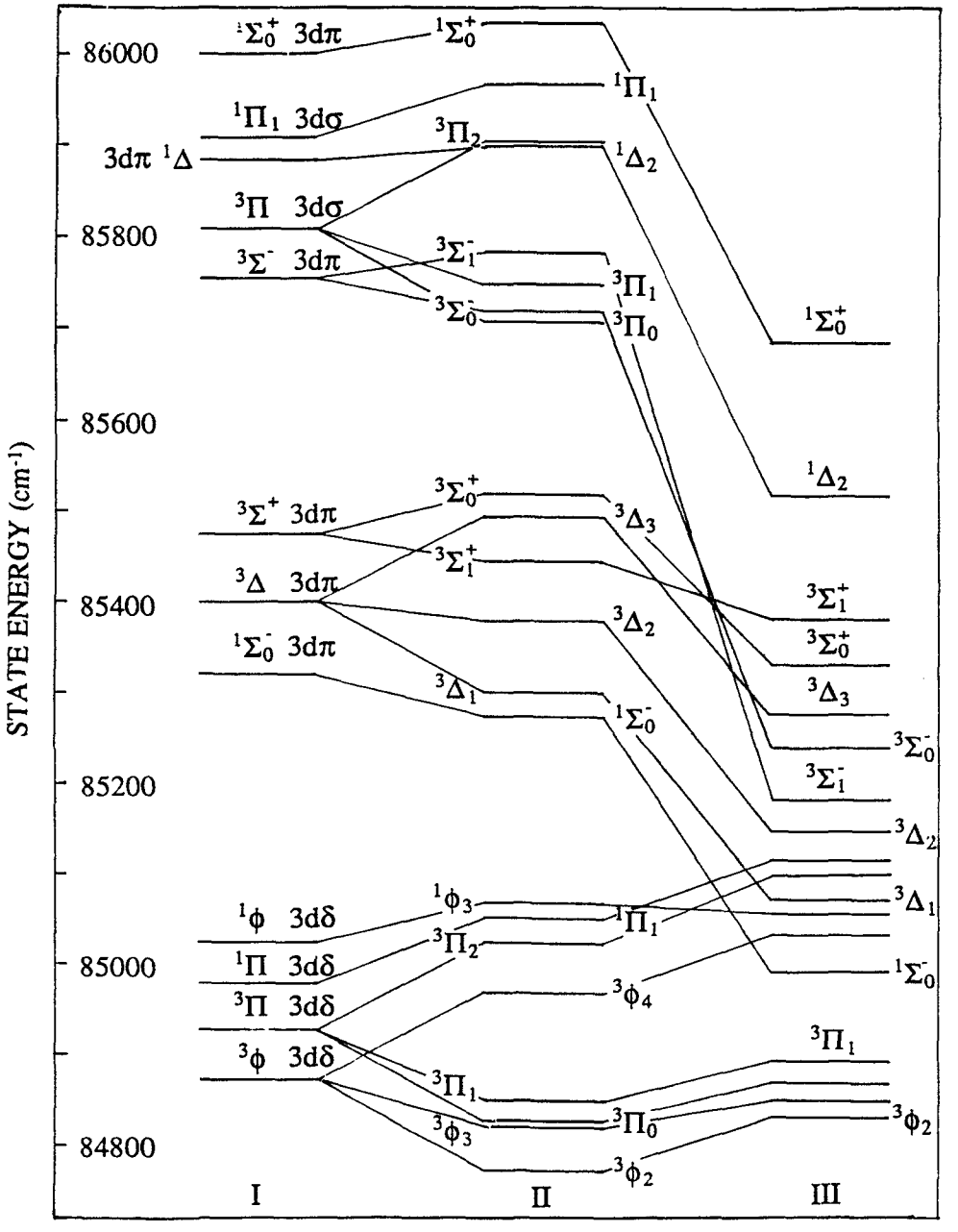

FIG. 1. Column I shows the calculated term energies without spin–orbit interactions for $v' = 0$ of the $3d\lambda$ Rydberg states. Column II shows the calculated state energies including spin–orbit coupling and column III shows the experimentally determined state energies.

tal values which we have determined to date. To avoid congestion, the figure does not show the $4s$ $v' = 1$ levels which have also been identified in this region.

In this work a large energy region was scanned which included the predicted locations of the following bands: 108 of the 110 bands due to the $v' = 0$–4 levels of the 22 $3d\lambda$ states, 44 of the bands due to the $v' = 0$–1 levels of the 22 $4d\lambda$ states, 20 of the bands due to the $v' = 0$–4 levels of the 4 $4s\sigma$ states, 8 of the bands due to the $v' = 0$–1 levels of the 4 $5s\sigma$ states, and the 4 bands due to the $v' = 0$ level of the 4 $6s\sigma$ states. We did not suceed in definitively locating all 184 of these bands due to spectral congestion compounded by peak broadening and suppression due to predissociation. Nevertheless, a sufficient number of these bands have been detected and reliably assigned so that the experimental energy levels shown in Fig. 1 can be accepted with confidence. The evidence for these assignments is presented in detail for each state.

Table I gives the values of band origins (obtained using independent wavelength calibration) for those bands which are now definitively located. In those cases where the assignment is considered very reliable but a complete rotational analysis has not been made, the entry is the energy of the strongest feature of the coldest spectrum of the band and it is marked with a *. The other entries in the table are the total energy of the rotationless level of the state. This convention was adopted because it was not always possible to perform a meaningful extrapolation to the sometimes nonexistent $J' = 0$ level.

Table II presents effective B' values or B' and γ values when the energy level expression included the effects of s uncoupling. In many cases these are rough values suggested by observation of less than five rotational levels. The numerous interactions between states would make it extremely difficult to achieve a more rigorous analysis of this extremely congested spectrum.

The ten states of the $3d\lambda$ manifold which appeared the strongest in the REMPI spectrum are the Δ and Σ states formed by populating the $3d\pi$ orbital. Therefore, the calculations concerned with these states will be described in some detail.

TABLE I. Band origins in cm^{-1}.

		$nd\delta\ ^{1,3}\phi$ states		
v'	$^3\phi_2$	$^3\phi_3$	$^3\phi_4$	$^1\phi_3$
0	84 835.4	84 858.2	85 038.1	85 060.9
1	86 714.3	86 737.1	86 916.6	86 939.2
2	88 560.4	88 582.9	88 762.3	88 784.3
3	90 374.7	90 396.7	⋯	⋯
		$nd\pi\ ^{1,3}\Delta$ states		
v'	$^3\Delta_1$	$^3\Delta_2$	$^3\Delta_3$	$^1\Delta_2$
0	85 076.0	85 151.3	85 280.3	85 522.4
1	86 944.3	87 019.3	87 148.1	87 390.8
2	88 779.5	88 855.1	88 982.8	89 225.2
3	90 582.3	90 657.8	90 785.0	91 027.0
4	92 352.6	92 426.7	92 554.6	⋯
1 ($4d$)	⋯	⋯	92 571.7	⋯
		$4s\sigma\ ^{1,3}\Pi$ states		
v'	$^3\Pi_0$	$^3\Pi_1$	$^3\Pi_2$	$^1\Pi_1$
0	83 361.0*[a]	83 373.2*	83 541.1*	(83 551.8*)
4	90 646.7	⋯	90 841.3	⋯
		$5s\sigma\ ^{1,3}\Pi$ states		
v'	$^3\Pi_0$	$^3\Pi_1$	$^3\Pi_2$	$^1\Pi_1$
0	89 717.1	89 730.1	89 916.6	(89 926.0)
1	91 621.0*	91 615.1*	91 797.6*	(91 809.0*)
		$nd\pi\ ^{1,3}\Sigma^-$ states		
v'	$^1\Sigma_0^-$	$^3\Sigma_1^-$		$^3\Sigma_0^-$
0	84 996.7*	85 181.9*		85 242.5
1	86 864.4*	87 047.6*		87 108.3
2	88 715.9*	88 883.6		88 940.9
3	⋯	90 684.9		90 740.7
4	⋯	92 452.2		92 507.5
0 ($4d$)	⋯	90 564.0*		90 604.2
1 ($4d$)	⋯	92 421.8*		92 474.8
		$^{1,3}\Sigma^+$ states		
v'	$^3\Sigma_0^+$	$^3\Sigma_1^+$		$^1\Sigma_0^+$
0	85 334.0*	85 384.6		85 689.2
1	87 202.7*	87 251.8		87 557.3
2	89 037.9*	89 085.3		89 393.0
3	90 840.5*	90 887.3		91 195.5
4	⋯	92 655.1		⋯
0 ($4d$)	⋯	90 749.4*		90 869.1
1 ($4d$)	⋯	92 617.4		92 739.7

[a] The asterik is used to indicate that the energy quoted is the energy of the strongest feature in the coldest spectrum of the band and not necessarily the origin.

TABLE II. Effective molecular rotational constants are presented for states first analyzed in this work.

		$nd\pi\ ^{1,3}\Delta$ states			
v'		$^3\Delta_1$		$^3\Delta_2$	$^3\Delta_3$
0		1.596		1.585	1.675
1		1.546		1.581	1.647
2		1.475		1.560	1.586
3		1.375		1.572	1.603
4		1.400		⋯	1.577
1 ($4d$)		⋯		⋯	1.550
		$4s\sigma\ ^{1,3}\Pi$ states			
v'	$^3\Pi_0$	$^3\Pi_2$			
4	1.453	1.569			
		$5s\sigma\ ^{1,3}\Pi$ states			
v'		$^3\Pi_0$	$^3\Pi_1$	$^3\Pi_2$	$^1\Pi_1$
0	B'	1.558	1.947	1.628	1.823
	γ	−0.6156	⋯	0.5556	⋯
		$3d\pi\ ^3\Sigma$ states			
v'		$^3\Sigma_1^-$		$^3\Sigma_0^-$	$^3\Sigma_1^+$
0		⋯		1.850	2.225
1		⋯		2.183	1.773
2		1.520		2.117	1.075
3	B'	1.583		2.233	⋯
	γ	−1.433		⋯	⋯
4		1.175		2.400	⋯
		$4d\pi\ ^{1,3}\Sigma$ states			
v'		$^3\Sigma_0^-$			$^1\Sigma_0^+$
0		2.067			1.867
1		1.933			1.807

Recknagel[3] showed how the terms resulting from a $\Pi\Pi'$ configuration can be described by three parameters a, b, and c which are related to Coulomb and exchange integrals. Recknagel's approach leads to the following equations for the first order state energies:

$$(5.1)\quad {}^3\Sigma^+ = E + a - b,$$

$$(5.2)\quad {}^3\Delta = E,$$

$$(5.3)\quad {}^3\Sigma^- = E + 2c - a - b,$$

$$(5.4)\quad {}^1\Sigma^- = E - a + b,$$

$$(5.5)\quad {}^1\Delta = E + 2c,$$

$$(5.6)\quad {}^1\Sigma^+ = E + 2c + a + b.$$

Field[4] extended this approach to include spin–orbit coupling. Including spin–orbit coupling, the states and their energies are given by the following equations:

$$(5.7)\quad {}^3\Delta_3, {}^3\Delta_1 = 0 \pm [(a_\pi + a'_\pi)/2]^{.5},$$

$$(5.8)\quad {}^1\Delta_2, {}^3\Delta_2 = c \pm (1/2)[a_\pi^2 + 4c^2]^{.5},$$

$$(5.9)\quad {}^3\Sigma_0^+, {}^1\Sigma_0^- = 0 \pm (1/2)[a_\pi^2 + 4(a-b)^2]^{.5},$$

$$(5.10)\quad {}^3\Sigma_1^-, {}^3\Sigma_1^+ = (c-b) \pm (1/2)[a_\pi^2 + 4(c-a)^2]^{.5},$$

$$(5.11)\quad {}^1\Sigma_0^+, {}^3\Sigma_0^- = 2c \pm (1/2)[a_\pi^2 + 4(a+b)^2]^{.5}.$$

For a Rydberg state a'_π is negligible and a_π is the spin–orbit splitting of the ion core. The energy zero is the average energy of the $^3\Delta_1$ and $^3\Delta_3$ states. The $\pm$ sign can be inverted and should be chosen so that the state with the highest first order energy is increased in energy.

In our previous work a set of Recknagel parameters was given which fit both the Σ and Δ states arising from the $3d\pi$ orbital quite well. Furthermore, these parameters could be scaled for $n = 4$ and 5 and gave a good fit to the available data there as well. The agreement between the calculated and experimental energy splittings is shown in Table III. Table IV shows the extent of state mixing calculated due to spin–orbit interaction.

The spectra and their assignments are now discussed for each state.

TABLE III. Comparison of the experimental energies with those calculated from the Recknagel parameters for the $nd\pi$ states for $v' = 0$.

State	Experimental relative energy	Calculated relative energy	ΔE (c–e)
	$3d\pi$ states		
$^1\Sigma_0^-$	− 181.5	− 155	26.5
$^3\Delta_1$	− 102.2	− 101	1.2
$^3\Delta_2$	− 26.9	− 30	− 3.1
$^3\Sigma_1^-$	2.4	1	− 1.4
$^3\Sigma_0^-$	64.3	64	− 0.3
$^3\Delta_3$	102.1	101	− 1.1
$^3\Sigma_0^+$	155.8	155	− 0.8
$^3\Sigma_1^+$	206.4	203	− 3.4
$^1\Delta_2$	344.2	330	− 14.2
$^1\Sigma_0^+$	511.0	536	25.0

Parameters			
a	b	c	a_π
166	48	150	200

State	Experimental relative energy	Calculated relative energy	C–E
	$4d\pi$ states		
$^3\Sigma_1^-$	− 47.9	− 57.2	− 9.3
$^3\Sigma_0^-$	5.1	− 8.5	− 13.6
$^3\Delta_3$	102.0	101.0	− 1.0
$^3\Sigma_1^+$	147.7	143.2	− 4.5
$^1\Sigma_0^+$	270.0	260.5	− 9.5

Parameters			
a	b	c	a_π
70	20	63	200

B. The $3d\pi$ $^1\Sigma_0^-$ state

In the earlier work it was pointed out that polarization experiments indicated that a barely detectable Σ-type band occurred near the calculated location of the $^1\Sigma_0^-$ band for $v' = 1$. At that time no other vibrational levels of this state had been detected. We have now located the $v' = 0$ and $v' = 2$ levels in addition to the $v' = 1$ level of this band. The $v' = 0$–2 levels are shown in Fig. 2. The presence of Q lines (which are definitively identified by the polarization experiments) is forbidden by the case (a)-case (b) two-photon rotational line strength factors for a $^3\Sigma_g^- \rightarrow\rightarrow (^1\Sigma_0^- \text{ or } ^3\Sigma_0^+)$ transition. The presence of these lines suggests the following mixing scheme. The $^1\Sigma_0^-$ state is mixed by spin–orbit coupling with the $^3\Sigma_0^+$ state. The latter state can mix by s uncoupling with the $^3\Sigma_1^+$ state which has a high degree of $^3\Sigma_1^-$ character. For the $^3\Sigma_1^-$ band the Q lines are strongly allowed. The identification of the $^1\Sigma_0^-$ band is important as evidence of s uncoupling in the Σ states for which it is difficult to observe many rotational levels due to predissociation and also as a check on the accuracy of the Recknagel calculations which strongly support our electronic assignments.

C. The $3d\pi$ $^3\Sigma_0^+$ state

This state, the pertubation partner of the $^1\Sigma_0^+$ state described above, is electronically assigned on the basis of the parameterized calculations summarized in Table III. The Recknagel parameters chosen to reproduce the energies of the strong Σ states predict that the $^3\Sigma_0^+$ state will lie within a few cm^{-1} of an observed polarization-sensitive band of low intensity also known in our earlier work as 3Σ. We have now located the $v' = 0$–3 levels of this state and the spectra are

TABLE IV. Mixing of pairs of $nd\pi$ states by spin–orbit coupling.

State pairs mixed	% Admixture
$^3\Sigma_1^+ - ^3\Sigma_1^-$	42%
$^3\Sigma_0^+ - ^1\Sigma_0^-$	12%
$^1\Delta_2 - ^3\Delta_2$	8%
$^3\Sigma_0^- - ^1\Sigma_0^+$	5%

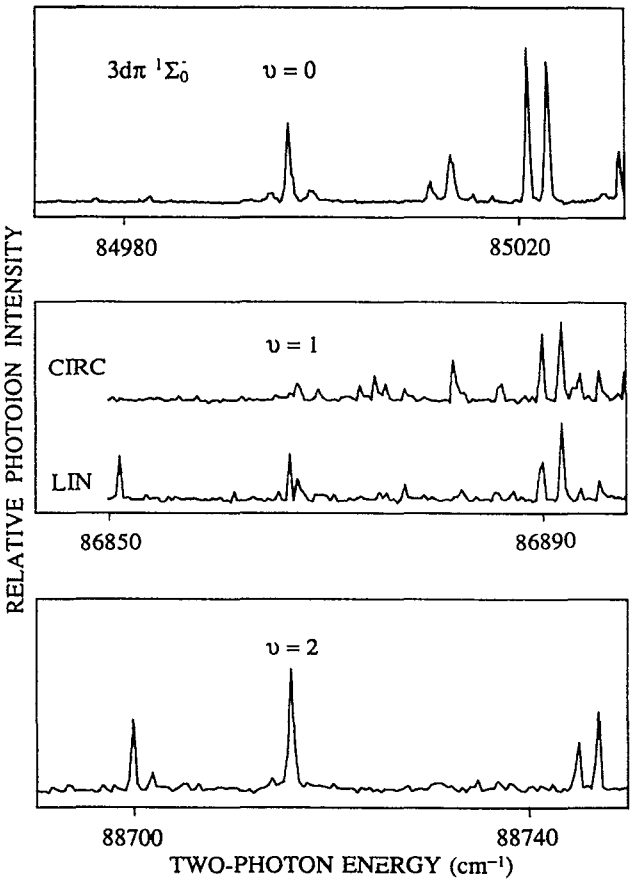

FIG. 2. The spectra for $v' = 0$–2 of the $3d\pi\ ^1\Sigma_0^-$ state are shown. For $v' = 1$ the polarization dependence of the spectra is shown and clearly identifies this as a Σ state. The intense peaks at the high energy end of the spectra, which are not affected by polarization change, belong to the $^3\phi_4$ state and are included to show their relative insensitivity to this change.

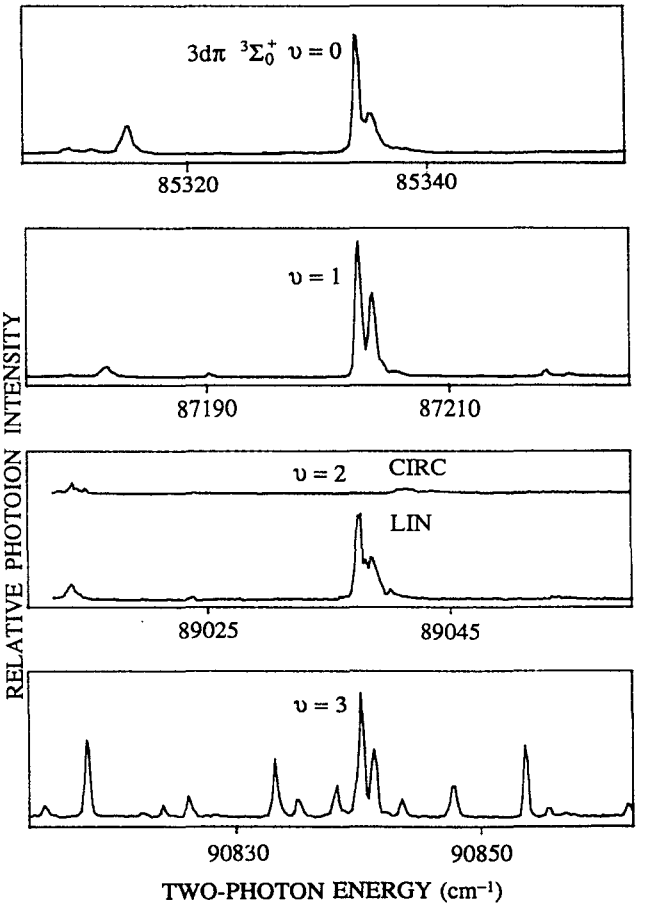

FIG. 3. The spectra for $v' = 0$–3 of the $3d\pi\ ^3\Sigma_0^+$ state are shown. The dramatic polarization dependence, shown for the $v' = 2$ level, clearly identifies this as a Σ state.

shown in Fig. 3. It can be seen in this figure that there are two strong Q lines in these bands, but very little additional rotational structure. The remarks on s uncoupling in Sec. III A apply to this state as well.

D. The $3d\pi\ ^1\Sigma_0^+$ state

This state is the easiest to detect and assign of all the Rydberg states of O_2 and the only new contribution in this work is the presentation of somewhat more accurate energies and eigenvectors. This state is surprisingly intense given the small amount of $^3\Sigma$ character in the Rydberg state. This is probably due to the fact that the state is the least predissociated of all the Σ states.

E. The $3d\pi\ ^3\Sigma_1^+$ state

The spectrum of this state is quite intense due to a large admixture of $^3\Sigma_1^-$ character. It is observed for the $3d\ v' = 0$–4 and $4d\ v' = 0$–1 levels. The $3d\ v' = 1$ band is the most readily analyzed despite evidence of predissociation. The analysis is shown in Fig. 4 along with the polarization data which support the assignment. The analysis of the $3d\ v' = 2$

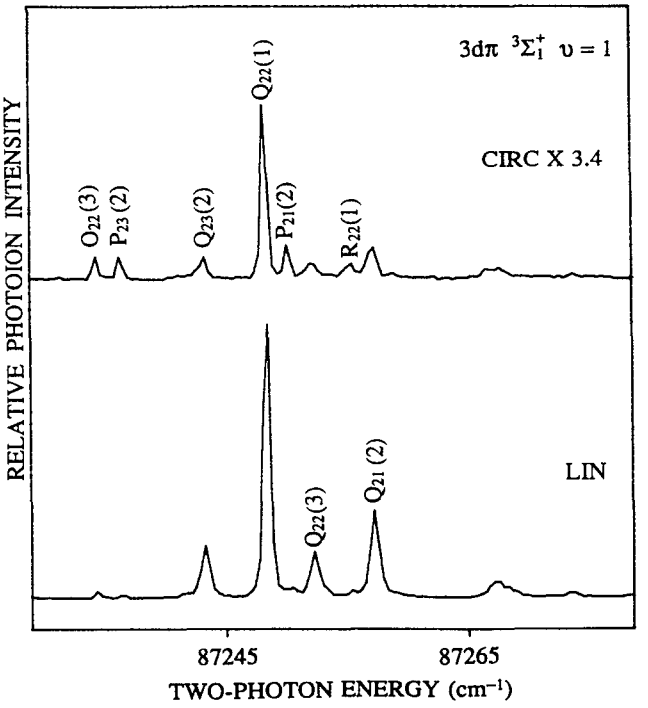

FIG. 4. The spectrum for $v' = 1$ of the $3d\pi\ ^3\Sigma_1^+$ state is shown in linear and circular polarization. The ordinate of the circular polarization spectrum is multiplied by a factor of 3.4 so that the smaller details can more readily be seen.

band is also fairly straightforward. This band along with the bands for $3d\ v' = 3$ and 4 and $4d\ v' = 1$ are shown in Fig. 5. Most of these bands consist of only a few strong lines presumably due to strong predissociation of higher rotational levels. The $4d\ v' = 0$ level (shown in a later figure) appears to be slightly less predissociated than the $4d\ v' = 1$ level, but is severely overlapped making a detailed comparison difficult. The $3d\ v' = 0$ band is overlapped by a large number of very broad peaks extending 65 cm^{-1} to the high energy side of the band center. These broad peaks are very probably due to the $v' = 1$ level of the $4s\sigma$ Π states (as will be discussed later) and do not overlap the $^3\Sigma_1^+$ band in the $^{18}O_2$ spectrum which, nonetheless, still shows strong heterogeneous predissociation indicated by rapid broadening and intensity decrease with increasing value of J. This effect can be seen in Fig. 6. It is concluded that predissociation of the $^3\Sigma_1^+$ is mainly *direct* as opposed to indirect predissociation[5] by the $4s\sigma$ Π states. However, the large change in effective B' values (Table II) for the $v' = 0$–2 levels of the $^3\Sigma_0^+$ state indicates that some v' dependent mixing with the $4s\sigma$ Π states may be occurring.

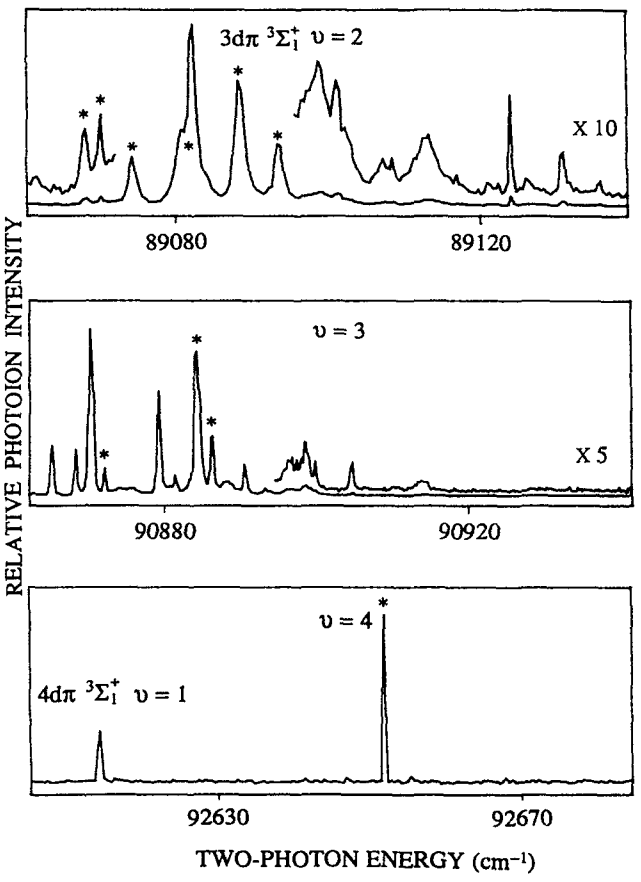

FIG. 5. The spectra for $v' = 2$, 3, and 4 of the $3d\pi\ ^3\Sigma_1^+$ state and $v' = 1$ of the $4d\pi\ ^3\Sigma_1^+$ state are shown. The peaks of the $3d\pi$ bands are marked with a *. Other lines in the spectra are due to overlapping $4s\sigma$ and $4d\pi$ bands.

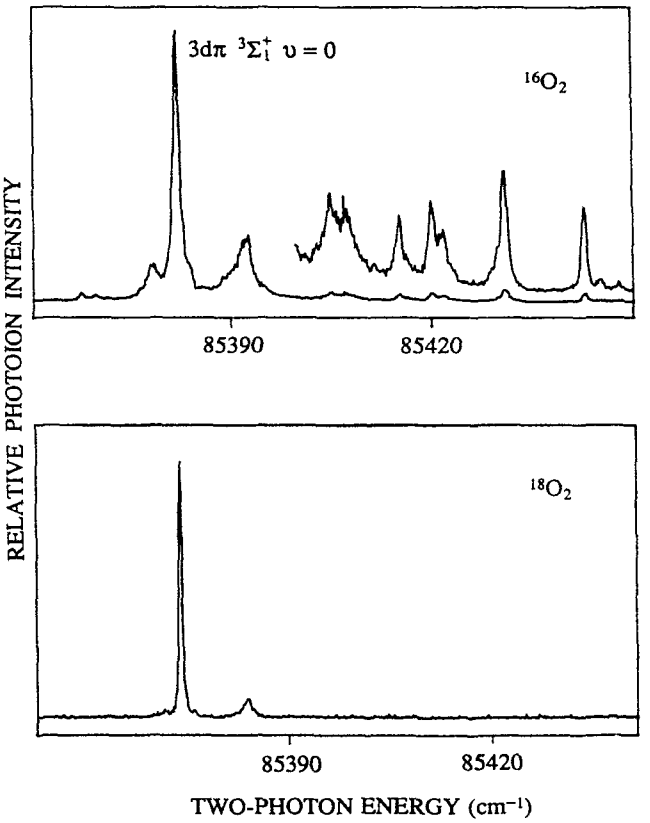

FIG. 6. The spectrum of $v' = 0$ of the $3d\pi\ ^3\Sigma_1^+$ state is shown for $^{16}O_2$ and $^{18}O_2$. Note the difference in linewidth for the two isotopes.

F. The $3d\pi\ ^3\Sigma_0^-$ state

This state is always seen as one of the most intense bands for the $3d\ v' = 0$–4 and the $4d\ v' = 0$ and 1 levels. All the levels are strongly heterogeneously predissociated with very noticeable J' dependence of the linewidths. The case (a)-case (b) two-photon rotational linestrength factors for a $^3\Sigma_g^- \rightarrow\rightarrow {}^3\Sigma_0^-$ transition forbid transitions from F_2'' levels and forbid P or R branches. Thus for all the levels except the $3d\ v' = 1$ level the rotational analysis is straightforward and can be seen in Figs. 7 and 8.

The $v' = 1$ band shows more Q lines than would be expected for this state alone. The evidence for this can be seen in the top two traces of Fig. 9 where the polarization data for this region is shown. These "extra" Q lines are more easily seen when the band is examined at higher power as shown in the third trace of Fig. 9. Finally, these extra Q lines disappear in the $^{18}O_2$ spectrum of this band which resembles the spectrum of the other less perturbed levels in $^{16}O_2$. The simplest explanation assumes that in $^{16}O_2$ the $v' = 1$ level of the $^3\Sigma_0^-$ state is strongly mixed with the $v' = 2$ level of a $4s\sigma$ Π state. The Π state levels have enough Σ character to make their Q lines polarization sensitive. There also may be some indirect predissociation due to this interaction as the Σ band has much greater rotational linewidths in the $^{16}O_2$ spectrum

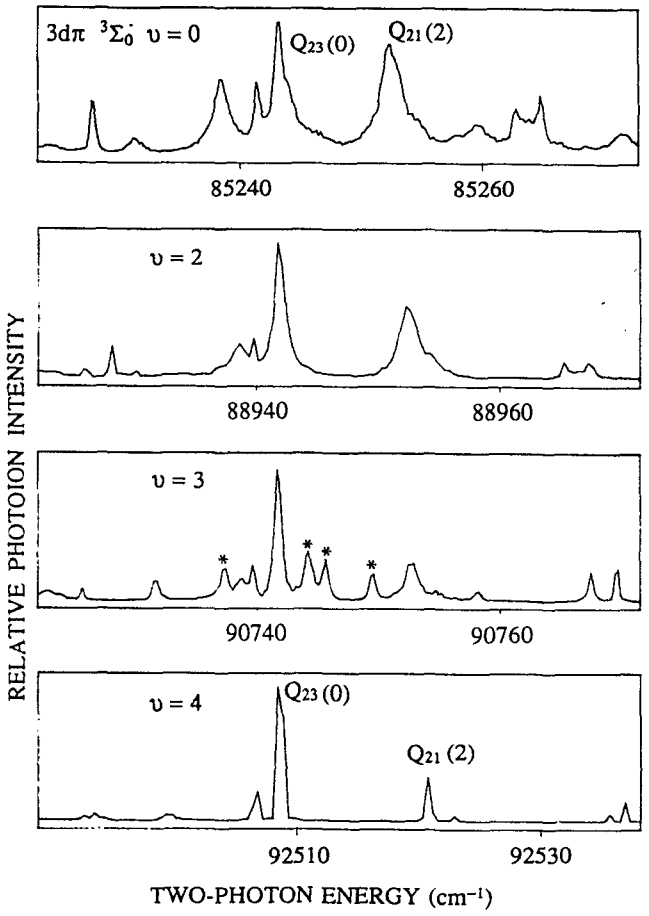

FIG. 7. The spectra for $v' = 0$ and 2–4 of the $3d\pi\ ^3\Sigma_0^-$ state are shown. The strong increase in blue shading and apparent concurrent drop in predissociation rate with v' are quite evident. The $v' = 3$ spectrum is overlapped by the $4d\pi\ ^3\Sigma_1^+$ $v' = 0$ band, these peaks being marked with *.

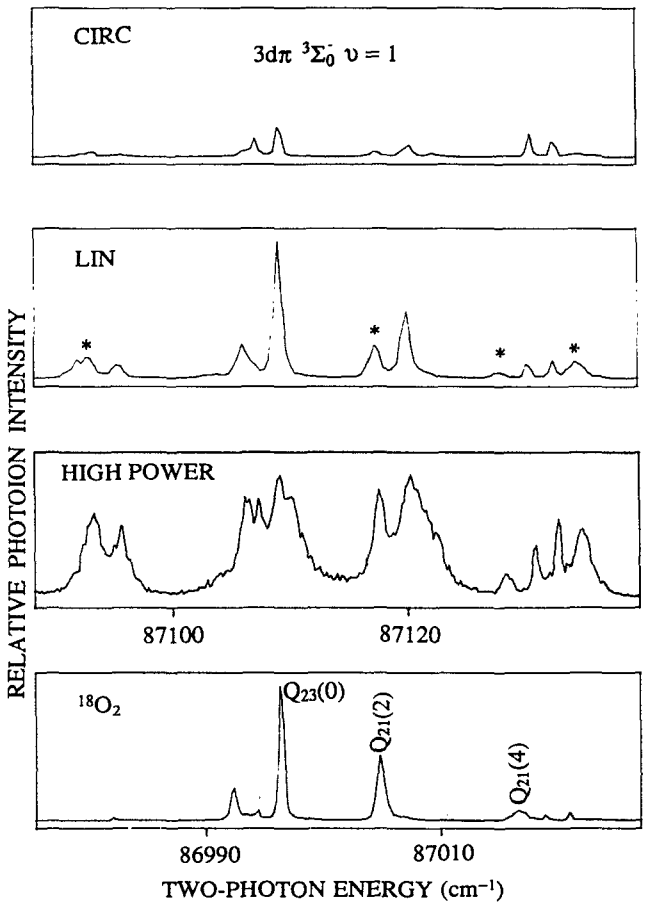

FIG. 9. The spectrum of $v' = 1$ of the $3d\pi\ ^3\Sigma_0^-$ state is shown taken under various experimental conditions. The top three traces (for $^{16}O_2$) all have identical energy scales to facilitate comparison of the data. The extra Q lines (see the text) are marked with *. The lowest spectrum is that of $^{18}O_2$.

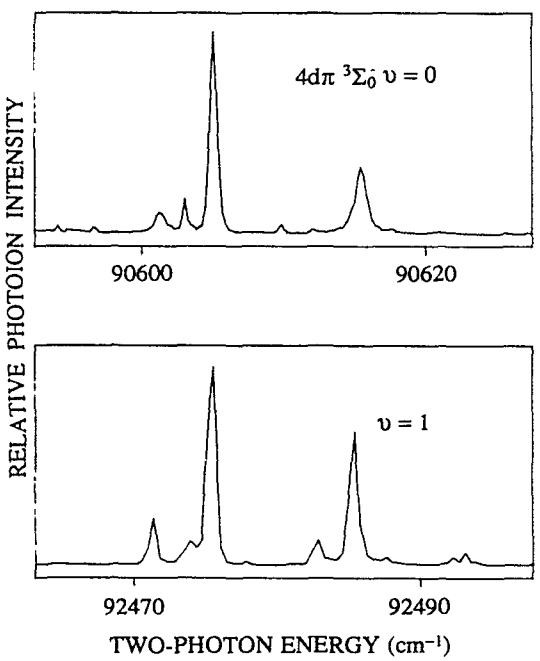

FIG. 8. The spectra for $v' = 0$ and 1 of the $4d\pi\ ^3\Sigma_0^-$ state are shown. All the expected levels of this state are observed and are intense. The rotational structures are very similar except for the $3d\pi\ v' = 1$ level in $^{16}O_2$ (see Fig. 9.)

than in the $^{18}O_2$ spectrum. In the $^{18}O_2$ spectrum the *direct* predissociation is very easy to see since overlap with the neighboring $^3\Delta_3$ band is reduced.

G. The $3d\pi\ ^3\Sigma_1^-$ state

One of the earliest bands studied in detail was the $v' = 2$ level of the $3d\pi\ ^3\Sigma_1^-$ state. It can be assigned convincingly on the basis of thermal data (see Fig. 2 of Ref. 1), polarization data (see Fig. 10), and the Recknagel calculations (see Table III). The spectra of the $3d$ $v' = 3$ and 4 levels are quite similar to the $v' = 2$ band as can be seen in Fig. 11. The spectra of the $4d$ $v' = 0$ and 1 levels of this state are considerably reduced in intensity and are also broadened, but nevertheless are definitively located on the basis of the polarization data (see Fig. 2 of Ref. 1).

In contrast, the $3d$ $v' = 0$ and 1 levels are very perturbed. For $v' = 1$ in linear polarization there are numerous broadened, unassigned lines (see Fig. 12). In circular polarization there are numerous weak but sharp peaks (see Fig. 12). Ground state combination differences corresponding to transitions from low J'' are not convincingly identified in the

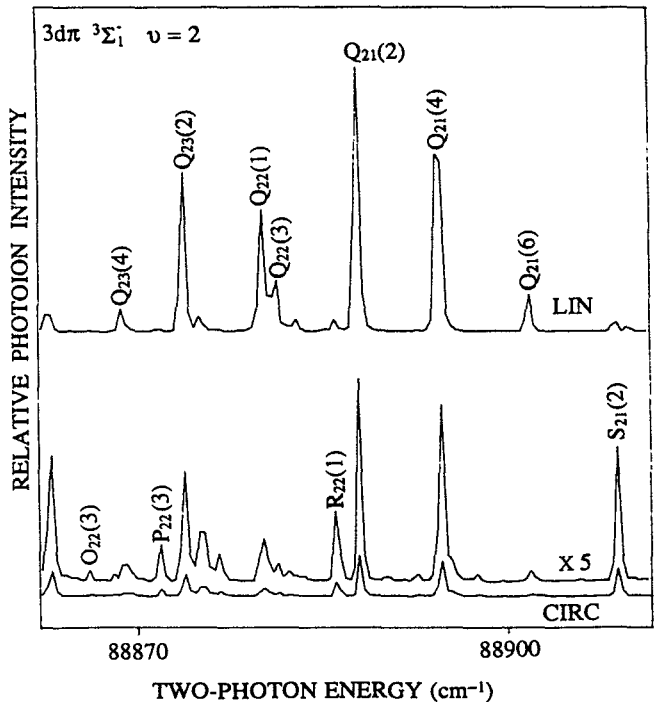

FIG. 10. The spectrum is shown for $v' = 2$ of the $3d\pi\ ^3\Sigma_1^-$ state. The rotational assignment is shown along with the polarization dependence that supports the assignment.

spectrum taken with either polarization. Nevertheless, the spectrum shows polarization dependence, and the line positions are the same when the laser power, ion channel (O_2^+ or O^+), or presence of the laser fundamental is varied. It was hoped that measuring the spectrum of this band in $^{18}O_2$ might finally enable an analysis, but the band turned out to be severely predissociated and only a few broadened, weak peaks were seen which are also not yet rotationally analyzed (see Fig. 12).

Even more dramatic is the apparent disappearance of the $v' = 0$ band at moderate powers as seen in Fig. 1 of Ref. 1. At first it was suspected that this was due to indirect predissociation by the $v' = 1$ level of one of the $4s\sigma\ \Pi$ states which must lie in this region. It was possible using enhanced detection sensitivity and increased laser power to find the $v' = 0$ level of the $4s\sigma\ ^3\Pi_0$ and $^3\Pi_1$ states about one vibrational interval below the $v' = 0$ level of the $3d\pi\ ^3\Sigma_1^-$ state (*vide infra*). Using the same experimental conditions some very broadened peaks due to the $v' = 0$ level of the $^3\Sigma_1^-$ state were found (see Fig. 13). In contrast to the very strong predissociation of the $^3\Sigma_1^-$ state, sharper, and much more intense, peaks belonging to the $^3\Sigma_0^-$ state (Fig. 7) lie only 50 cm^{-1} away. This circumstance suggested that the great difference in predissociation rate might best be explained by invoking indirect predissociation by the $v' = 1$ level of one of the $4s\sigma$

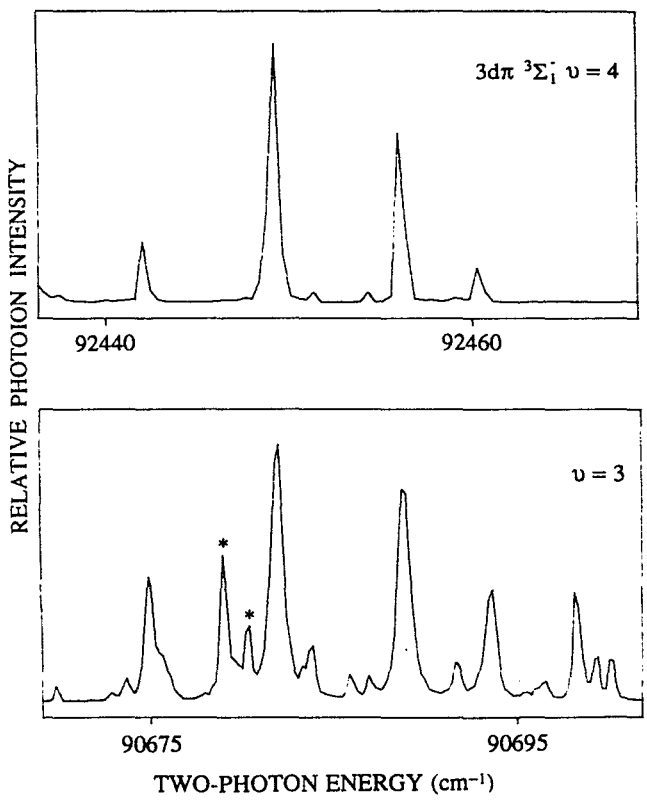

FIG. 11. The spectra for $v' = 3$ and 4 of the $3d\pi\ ^3\Sigma_1^-$ state are shown. These bands are intense, analyzed, and quite similar to the $v' = 2$ band shown in Fig. 10. The $v' = 3$ band is overlapped by the $3d\pi\ ^3\Delta_2$ $v' = 3$ band whose peaks are marked with a *. The $v' = 4$ level of $^3\Delta_2$ was not detected, presumably due to strong predissociation.

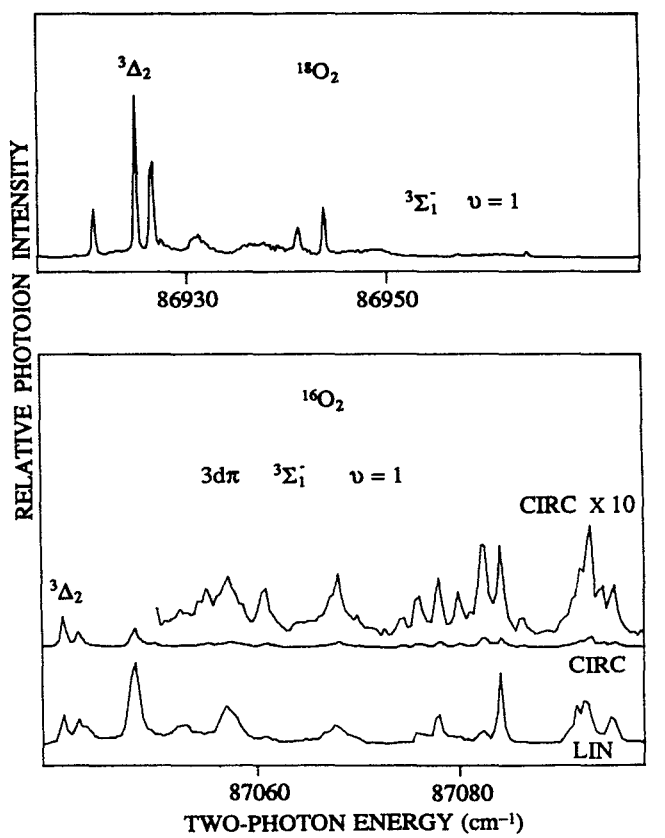

FIG. 12. The spectrum for $v' = 1$ of the $3d\pi\ ^3\Sigma_1^-$ state and part of the overlapping $3d\pi\ ^3\Delta_2$ band is shown for $^{16}O_2$ and $^{18}O_2$. In the $^{18}O_2$ spectrum all the sharp peaks are readily assigned to the $^3\Delta_2$ band.

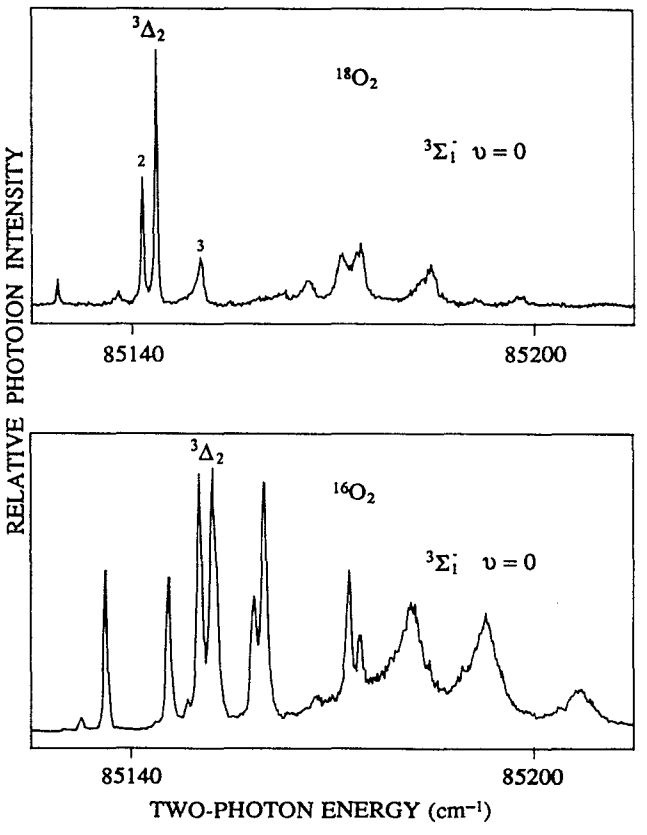

FIG. 13. The spectrum is shown for $v' = 0$ of the $3d\pi\ ^3\Delta_2$ and $^3\Sigma_1^-$ states in $^{16}O_2$ and $^{18}O_2$. The $^{16}O_2$ trace shows sharp peaks due to the $^3\Delta_2$ band and three broad peaks due to the $^3\Sigma_1^-$ band. The $^{18}O_2$ trace shows pronounced heterogeneous predissociation of the $^3\Delta_2$ band which is indicated by giving the value of J' for representative $^3\Delta_2$ peaks.

repulsive $1\ ^1\Pi_g$ and $1\ ^3\Pi_g$ valence states is probably responsible for most effects.

H. The $ns\sigma$ Π states: Identification and linewidths

The $3s\sigma$ Π states were the first gerade Rydberg states observed for O_2, initially by inelastic electron scattering[6,7] and more recently by two-photon REMPI.[8,9] The drastic variation in linewidths with vibrational quantum number for the $^3\Pi$ states was ascribed to predissociation by the $1\ ^3\Pi_g$ valence state and was used by Friedman and Dalgarno to fine tune the relative positions of the calculated Rydberg and valence state potential curves[10] and to determine the strength of the Rydberg–valence interaction.[11]

Earlier attempts to detect higher members of the $ns\sigma$ series were unsucessful.[2,4,12–14] This lack of sucess was attributed to predissociation as well as possibly a lower two-photon excitation probability as compared with excitation of the more intense members of the $3d\lambda$ Rydberg states. (It should be noted that the available laser power in the region of the $4s\sigma$ states is at best about 1 mj/pulse as compared with up to 30 mj/pulse in the region of the $3s\sigma$ states.)

Linewidth information for the higher $ns\sigma$ Π states is very desirable although interpretation is more complex due to Rydberg–Rydberg interactions and the fact that both the $1\ ^3\Pi_g$ and the $1\ ^1\Pi_g$ valence states now can play a part as shown in Fig. 14. In the present work using higher laser power, improved ion collection, and more signal averaging we were able to detect the $ns\sigma$ Π states and get linewidth information for states with $n = 4$ and 5.

The location of the $4s\sigma$ bands can be determined most precisely for $v' = 0$ and $v' = 4$. For $v' = 0$ the $4s\sigma$ Π states appear as two pairs of bands separated approximately by the spin–orbit splitting of the ion. The lower pair of bands is Π states which itself is expected to be strongly homogenously predissociated. For the $^{18}O_2$ isotope, the $4s\sigma\ ^3\Pi_0$ and $^3\Pi_1$ $v' = 1$ bands are expected to be shifted by about 88 cm^{-1} to the red relative to the $3d\pi\ ^3\Sigma_1^-$ $v' = 0$ band. Such a shift should eliminate any such accidental predissociation. As will be seen later the $4s\sigma\ ^3\Pi_2$ and $^1\Pi_2$ $v' = 1$ band should still be about 150 cm^{-1} away to the blue and should have no effect. Portions of the $3d\ v' = 0$ and 1 spectrum were scanned using $^{18}O_2$ and evidence for the expected shift was found. In $^{18}O_2$ the $v' = 0$ level of the $3d\pi\ ^3\Delta_2$ state, which is just to the red of the $v' = 0$ level of the $^3\Sigma_1^-$ state, showed much stronger heterogeneous predissociation than in $^{16}O_2$ (see Fig. 13). In $^{18}O_2$ the $v' = 1$ level of the $^3\Delta_2$ band is sharper than in $^{16}O_2$ (see Fig. 12). The observed changes in the predissociation rate of the $^3\Delta_2$ state in our isotope experiments are almost certainly due to changes in the mixing between the $^3\Delta_2$ state and nearby heavily predissociated Π states. Therefore, it seems likely that the expected isotope shift occurs. Despite this, for both $v' = 0$ and $v' = 1$ in $^{18}O_2$, the $3d\pi\ ^3\Sigma_1^-$ band is nearly undetectable and the spectra of these bands have no sharp peaks. Thus while some enhancement by indirect predissociation may occur, simple direct predissociation by the

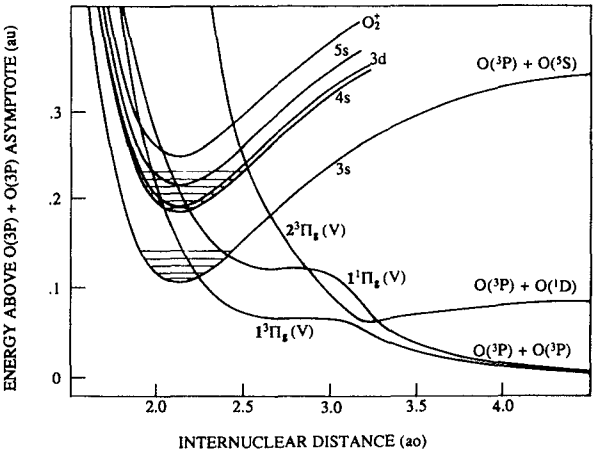

FIG. 14. Potential curves relevant to this study are shown. The potential curves of the $3s\sigma\ C\ ^3\Pi_g$ Rydberg state and the $1\ ^3\Pi_g$ valence state were taken from Fig. 1 of Ref. 8. The other Rydberg state curves were taken to be identical to that of the C state but displaced upward to agree with experiment. The additional two valence state curves were placed relative to the $1\ ^3\Pi_g$ curve using the calculations of Liu and Saxon. It can be seen that the highest levels we studied may interact with the $2\ ^3\Pi_g$ valence state.

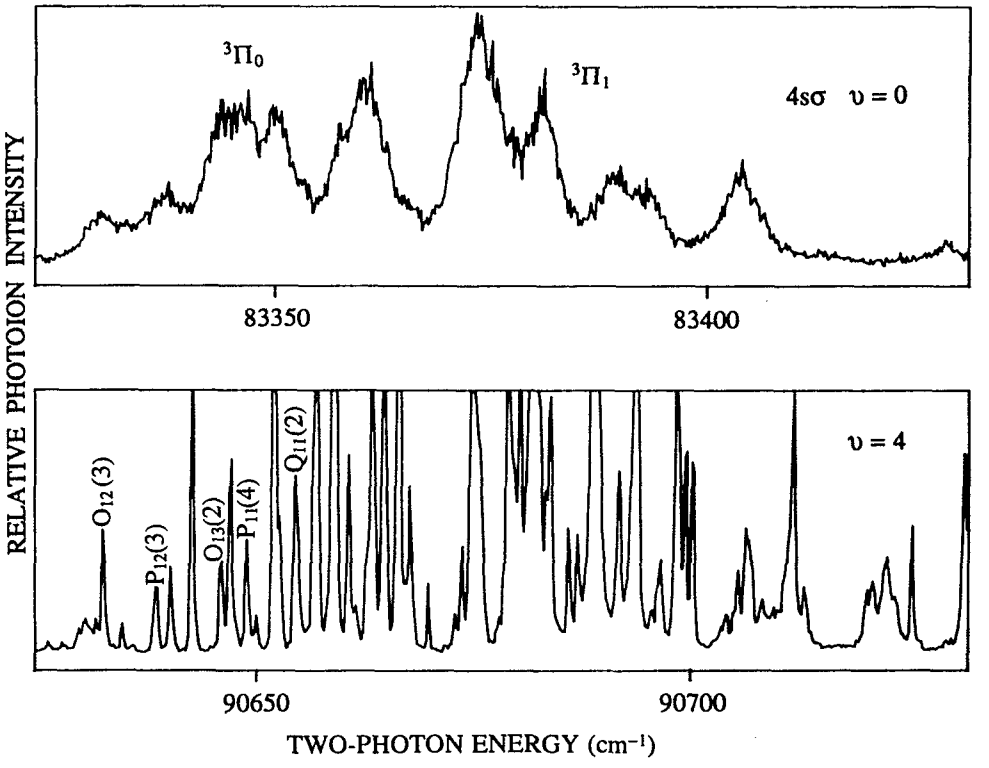

FIG. 15. The spectra for $v' = 0$ and 4 of the $4s\sigma\ ^3\Pi_0$ and $^3\Pi_1$ states are shown. The $v' = 0$ bands are isolated. The $v' = 4$ bands are overlapped by the much more intense $3d\pi\ ^3\Delta_2$ and $^3\Sigma_1^-\ v' = 3$ bands. The assignment for some of the $v' = 4$ peaks is shown.

composed of the $4s\sigma\ ^3\Pi_0$ and $^3\Pi_1$ states which converge to the lower spin–orbit component of the ion. The upper pair of bands is composed of the $4s\sigma\ ^3\Pi_2$ and $^1\Pi_1$ states which converge to the upper spin–orbit component of the ion. All four of these bands exhibit pronounced broadening, (evidently homogeneous), of the rotational lines (see Figs. 15–17). [The upper pair of bands is partially overlapped by $X\ ^3\Sigma_g^-$ $(v'' = 1) \rightarrow \rightarrow 3d\lambda$ $(v' = 0)$ transitions and these transitions account for all the sharp features in this energy region.] Due to the homogeneous broadening of the $4s\sigma\ \Pi$ states nearly all

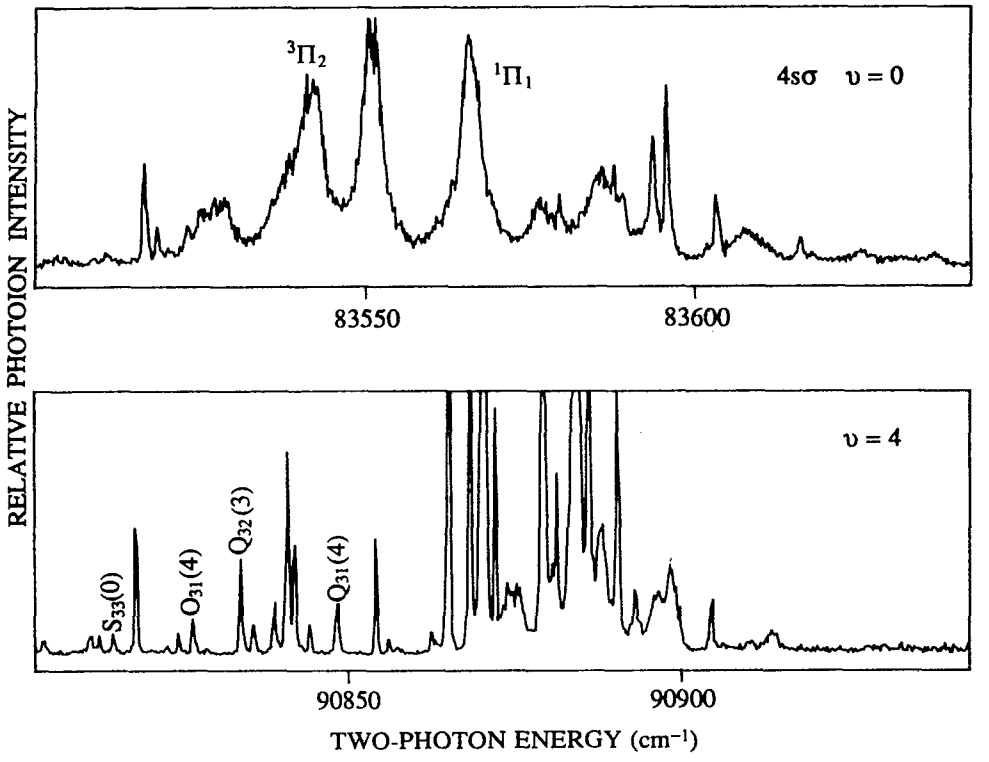

FIG. 16. The spectra for $v' = 0$ and 4 of the $4s\sigma\ ^3\Pi_2$ and $^1\Pi_1$ states are shown. All the sharp peaks in the $v' = 0$ spectrum belong to the $3d$ hotband as explained in the text. The $v' = 4$ bands are overlapped by the $3d\pi$ $(v' = 3)\ ^3\Delta_3$, $^3\Sigma_0^+$, and $^3\Sigma_1^+$ bands as well as the $4d\pi$ $(v' = 0)\ ^1\Sigma_0^+$ band. Some of the tentative assignments for the $v' = 4$ peaks are given.

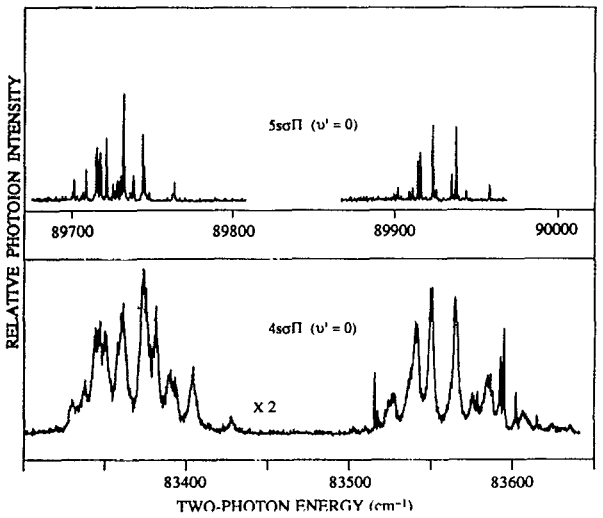

FIG. 17. The cold spectrum of the $4s\sigma\ \Pi$ ($v' = 0$) bands is shown aligned with the cold spectrum of the $5s\sigma\ \Pi$ ($v' = 0$) bands. The intensity of the lower energy half of the 4s spectrum is multiplied by a factor of 2 to better show the details. It can be seen that the main features of the 4s and 5s states line up quite well.

the features in their spectrum are composite features and we do not have a rotational analysis for these bands at this time. However, there are several isolated features in these bands which are probably single rotational lines and we measure their width to be $\approx 3.2\ \text{cm}^{-1}$ (FWHM).

As stated previously $v' = 4$ is the other level for which the $4s\sigma\ \Pi$ states can be most precisely located and characterized. One can calculate the expected location of the $4s\sigma\ ^3\Pi_0$ ($v' = 4$) band by using the vibrational intervals of the ion which are nearly the same as those of the Rydberg states. In the predicted location of this band there is only one other overlapping band the $3d\pi\ ^3\Delta_2$ ($v' = 3$) band. No other bands are predicted to lie here. Our spectrum of this energy region shows that in between the intense features due to the $^3\Delta_2$ band are a number of small but sharp peaks (see Fig. 15). These peaks are not readily assigned to the $^3\Delta_2$ band, but they can all be readily assigned to a $^3\Pi_0$ band as shown in Fig. 15. Furthermore, these peaks line up in a suggestive manner with those of the $4s\sigma\ ^3\Pi_0$ ($v' = 0$) band which can also be seen in Fig. 15. The alignment shown in Fig. 15 implies a ($v' = 4$)–($v' = 0$) vibrational spacing for the $4s\sigma\ ^3\Pi_0$ state within a few cm^{-1} of that of the ion. For the reasons outlined above we feel fairly confident about the location of the $4s\sigma\ ^3\Pi_0$ ($v' = 4$) band and we measure the rotational linewidths to be $\approx 0.5\ \text{cm}^{-1}$.

The energy region where one would expect the $4s\sigma\ ^3\Pi_1$ ($v' = 4$) band is occupied by the very dense spectrum of the $3d\pi\ ^3\Sigma_1^-$ ($v' = 3$) band. This precludes any conclusions about this band on the basis of our data.

Slightly less than $200\ \text{cm}^{-1}$ higher in energy than the $4s\sigma\ ^3\Pi_0$ ($v' = 4$) band there is another group of small sharp peaks which cannot be assimilated into the analysis of the nearby well-characterized *nd* Rydberg states. These peaks fit an analysis as $^3\Pi_2$, but their spacing relative to the $4s\sigma\ ^3\Pi_0$ ($v' = 4$) band is about 5–10 cm^{-1} less than the $4s\sigma\ ^3\Pi_2$–$^3\Pi_0$ spacing for $v' = 0$ as shown in Fig. 16. It is possible that these peaks belong to a Π state formed by populating the $3d\sigma$ or $4d\sigma$ orbitals, but no other band associated with either of these orbitals has yet been definitively located in our work. We tentatively assign these peaks to the $4s\sigma\ ^3\Pi_2$ ($v' = 4$) band and suggest that a small ($\approx$5–10 cm^{-1}) vibrational level shift may be occurring. In the $3s\sigma\ \Pi$ states much larger vibrational level shifts ($< 150\ \text{cm}^{-1}$) are seen and are due to an interaction with the repulsive $1\ ^3\Pi_g$ valence state which also broadens the rotational lines.[9–11] If our assignment of the $4s\sigma\ ^3\Pi_2$ ($v' = 4$) band is correct then the narrow linewidths ($0.5\ \text{cm}^{-1}$) may preclude a vibrational level shift which occurs by the same mechanism as in the $3s\sigma\ \Pi$ states.

The energy region in which the $4s\sigma\ ^1\Pi_1$ ($v' = 4$) band would occur is occupied by numerous peaks due to *nd* Rydberg states and we cannot locate any peaks definitely due to the $4s\ ^1\Pi$ state.

Since the $v' = 0$ level of the 4s states is about one vibrational interval below the $v' = 0$ level of the 3d states, one expects each $v' > 0$ level of the 4s states to be overlapped by the $v' - 1$ level of the 3d states. Therefore, the $v' = 1$–3 levels of the $4s\sigma$ states are seen in our spectra primarily in the form of broadened structure underlying the more intense peaks of the $v' = 0$–2 levels of the 3d Rydberg states. The broadened structure tends to be centered around the expected location of the $4s\sigma\ \Pi$ levels and for each vibrational level it shifts about $30\ \text{cm}^{-1}$ to the red relative to the 3d states as would be expected. The observed broad peaks can be due to transitions to the $4s\sigma\ \Pi$ states or in some cases to transitions to levels of the 3d states which are strongly mixed with the $4s\sigma\ \Pi$ states and thus indirectly predissociated. One can differentiate between the two cases with some reliability by noting the ratio of O^+ to O_2^+ for these peaks. It has been experimentally determined that the O^+/O_2^+ ratio is the highest for Σ states, about 50% less for Δ states, and at least 90% less for ϕ and Π states. (These differences are probably a result of significant differences in ionic vibrational distributions due to differing probabilities of accessing the shape resonance in the ionization continuum at the three photon level.)[15]

Upon examination of the broad features in the spectral regions where the 4s $v' = 1$–3 bands are overlapped by the 3d $v' = 0$–2 bands it is apparent from the O^+/O_2 ratio that most of these features correspond to J' levels which are predominantly Σ in character. However, for each level ($v' = 1$–3) of the 4s states one can find at least one broadened peak associated with very little atomic oxygen ion production and very likely attributable to v', J' levels of the $4s\sigma\ \Pi$ states. For these features we measure the following widths: $v' = 1$, 2.5 cm^{-1}; $v' = 2$, 1.4 cm^{-1}; and $v' = 3$, 1.6 cm^{-1}. The value for $v' = 3$ is based on a single peak which may be a composite feature so that the true width may be closer to 0.8 cm^{-1}.

One would expect the $5s\sigma\ \Pi$ states to be less intense and less predissociated than the $4s\sigma\ \Pi$ states. This trend can be seen in Fig. 17 where the cold spectrum of the $4s\sigma\ \Pi$ ($v' = 0$) bands is lined up with the cold spectrum of the $5s\sigma\ \Pi$ ($v' = 0$) bands.

The spectra of the $v' = 0$ and $v' = 1$ levels of the $5s\sigma\ \Pi$ states are virtually identical and we could not detect a v' dependence of the linewidths. Both levels exhibit a tendency for the $^3\Pi_1$ and $^1\Pi_1$ peaks to be broader and less intense than those of the $^3\Pi_0$ and $^3\Pi_2$ states. This is one of several observations that seem to indicate that the states with more singlet character are the most heavily predissociated states at the higher energies ($> 89\,500\ cm^{-1}$) studied. This in turn implies that the $1\ ^1\Pi_g$ repulsive valence state is responsible for most of the predissociation at these higher energies. The average linewidth for the $5s\sigma\ ^3\Pi_0$ and $^3\Pi_2$ states is $0.5\ cm^{-1}$ as compared with $0.7\ cm^{-1}$ for the $^3\Pi_1$ and $^1\Pi_1$ states.

Part of the rotational analysis for the $5s$ states can be seen in the warm spectra shown in Figs. 18 and 19. A term proportional to J' is necessary in the energy level formula and the proportionality constant γ is about 1/3 of the B' value which is indicative of strong s uncoupling. We do not see evidence of "Λ doubling" in the spectra of the $5s\sigma\ \Pi$ states.

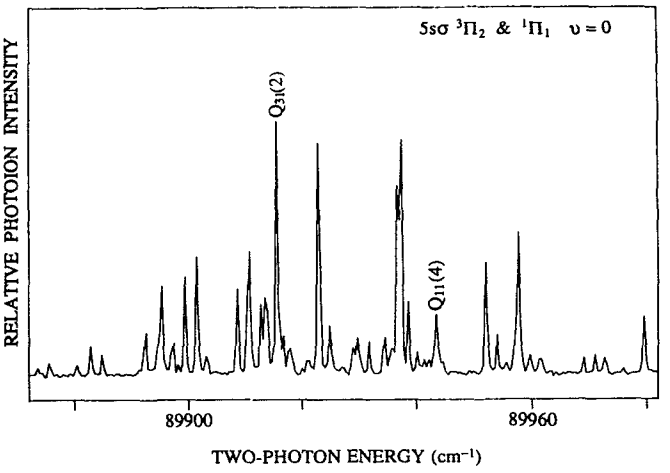

FIG. 19. The warm spectrum for $v' = 0$ of the $5s\sigma\ ^3\Pi_2$ and $^1\Pi_1$ states is shown and the strongest peak in each band is labeled to facilitate comparison of intensities and linewidths.

I. Intensities of the $ns\sigma\ \Pi$ states

The spectrum of the $4s\sigma$ ($v' = 0$) bands shown in Figs. 16 or 17 supports the earlier speculation that the low signal intensity of these states is due both to strong predissociation as well as low two-photon excitation probability as compared with that of the $3d$ states. This can be inferred by comparing the intensities of the $X\ ^3\Sigma_g^-$ $(v'' = 1) \rightarrow \rightarrow 3d\pi\ ^3\Delta_2$ $(v' = 0)$ "hot band" transitions with the intensities of the $X\ ^3\Sigma_g^-$ $(v'' = 0) \rightarrow \rightarrow 4s\sigma\ \Pi$ $(v' = 0)$ transitions. The intensities of the two types of transitions are comparable despite the fact that the transitions to the $3d$ states result from probing the small fraction (0.001) of thermally vibrationally excited molecules in the beam. (Vibrational cooling in the supersonic expansion is expected to be negligible in this case due to the high vibrational frequency of O_2.) The shorter lifetime of the $4s$ states can account for only 10^{-1} to 10^{-2} of this factor leading to the conclusion that the two-photon transition probability is probably at least 1 order of magnitude less than that of the $3d\pi\ ^3\Delta_1$ and $^3\Delta_2$ states whose bands are not the most intense features in the $3d\lambda$ spectrum.

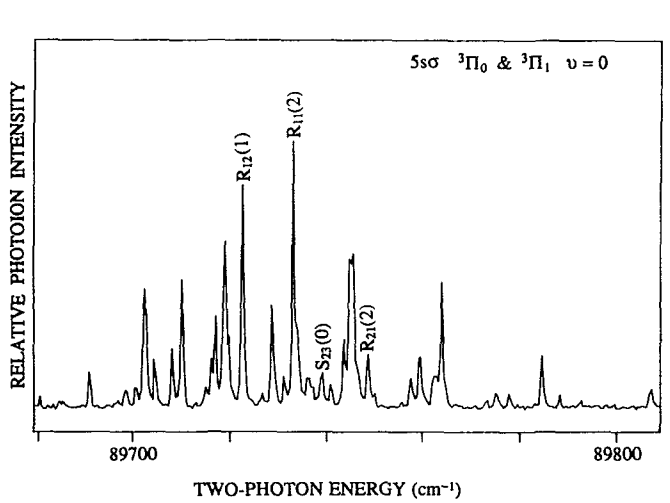

FIG. 18. The warm spectrum for $v' = 0$ of the $5s\sigma\ ^3\Pi_0$ and $^3\Pi_1$ states is shown and the two strongest lines in each band are labeled to facilitate comparison of intensities and linewidths.

J. Π states—Structural trends in the $ns\sigma$ series

The lowest members of the $ns\sigma$ series, the $3s\sigma\ \Pi$ states, are well described by an L–S coupling scheme and exhibit a singlet–triplet splitting[4,9] with an average value of $624\ cm^{-1}$, which is considerably larger than the $200\ cm^{-1}$ splitting of the ion core. In contrast the $4s$ and $5s$ states are more aptly described by a j–j coupling scheme and show two pairs of bands separated by the spin–orbit splitting of the ion core. For the $3s$ and $4s$ states the singlet–triplet splitting scales very roughly as $(n^*)^{-3}$.

For the $3s$, $4s$, and $5s$ states the quantum defects are 1.139, 1.1999, and 1.2078, respectively. There is a large change between $n = 3$ and 4, but only a small change between $n = 4$ and 5. The relative changes in these values are strikingly similar to those seen in the $ns\sigma$ Rydberg series of NO (Ref. 16) and are probably due to the same mechanism. The $4s\sigma$ and $5s\sigma$ states can be pushed to a lower energy through an interaction with the nearby $3d\sigma$ and $4d\sigma$ states respectively whereas the $3s\sigma$ state has no $(n-1)d\sigma$ state to repel it.

K. Higher energy levels of the Δ and φ states

Using our improved experimental sensitivity we were able to detect many previously unlocated or unidentified bands due to the $3d\lambda\ v' = 3$ and 4 levels and the $4d\lambda\ v' = 0$ and 1 levels. These levels are difficult to analyze because, due to the accidental overlapping, as many as 48 bands may lie in a $900\ cm^{-1}$ energy region. Most of the strongest bands can

be nicely rotationally assigned as seen in Tables I and II. However, in some cases there are regions with numerous peaks both sharp and broad in a melange which could belong to any of a number of bands expected to occur there. There is no doubt that the ongoing painstaking analysis of these regions will lead to more assignments. For example, it is now clear that the band marked "*A*" in Fig. 2 of Ref. 1 and tentatively assigned as the $4d\pi\ ^3\Delta_1$ ($v' = 0$) band is actually due to the $v' = 4$ level of the $3d\pi\ ^3\Delta_1$ state. The bands which have been successfully located to date are included in Table I.

Some useful conclusions can already be reached from the study of these higher energy levels. Most importantly, we have experimentally verified the accuracy of the Recknagel parameters for the $4d\pi$ states as can be seen in Table III. It is seen that these parameters scale as $(n^*)^{-3}$ in the expected manner. Quantum defects can be calculated for the *nd* states for $n = 3$ and 4 and are given in Table V. The general compression of the $nd\lambda$ spectrum as it converges with increasing n to the ground state of the ion can be seen plainly. Finally, it is clear, as mentioned earlier, that the high energy states which can mix most strongly with the $1\ ^1\Pi_g$ valence state are the most reduced in relative intensity. For example, in our data we cannot definitively locate a $^1\Delta_2$ or a $^3\Delta_2$ band for $4d$ $v' = 0$ or 1. On the other hand the $^3\Delta_3$ band is convincingly located for $4d$ $v' = 1$ and has moderate intensity.

L. The $3d\delta$ Π states

Ab initio calculations[2] place the spin–orbit components of the $3d\delta$ Π states to be about 55 cm^{-1} higher in energy than the corresponding spin–orbit components of the $3d\delta\ \phi$ states as can be seen in Fig. 1. In our work at moderate laser powers we saw no evidence of these states. Using the most intense laser powers we find that for $v' = 0$–2 there is a pronounced broad hump spanning approximately 75 cm^{-1} underlying the $3d\delta\ ^3\phi_3$ band. This structure can be seen in Fig. 20 which can be compared with Fig. 9 of Ref. 1 where the structure is not seen in the spectrum taken at moderate power. We assign this structure as due to the strongly homogeneously broadened $3d\delta\ ^3\Pi_0$ and $^3\Pi_1$ states. Since a rotational analysis is out of the question it is only possible to estimate the location of these origins.

One expects to find the upper pair of bands due to the $3d\delta$ Π states approximately 200 cm^{-1} to the blue of the lower pair, but for $v' = 0$ this location is occupied by relatively intense peaks due to the $^3\Delta_1$ state. However, slightly to the blue there are broadened residuals which are not assigned to any Δ or ϕ states. It can be seen in Fig. 21 that these broadened residuals occur at approximately the $3d$ vibrational spacing for $v' = 0$–2. There may be some small level shifts occurring, but the structure is too sparse to be certain of this. A plausible electronic assignment for these peaks ascribes them to the $3d\delta\ ^3\Pi_2$ and $^1\Pi_1$ states. In summary, though we do not have a rotational analysis for any $3d\delta$ Π state it seems

TABLE V. Quantum defects (δ) for selected states studied in this work, calculated using $X\ ^2\Pi_{1/2}(v' = 0) = 97\,348\ cm^{-1}$ and $X\ ^2\Pi_{3/2}(v' = 0) = 97\,548\ cm^{-1}$. In those cases where the calculation is based on a vibrational level other than $v' = 0$ the appropriate vibrational energy is added to the ion state and the entry in the table is followed by the vibrational level used in parentheses.

State	δ	State	δ
$3d\delta\ ^3\phi_2$	0.038 56	$4d\pi\ ^3\Sigma_1^-$	− 0.021 92
$3d\delta\ ^3\phi_3$	0.035 86	$4d\pi\ ^3\Sigma_0^-$	− 0.033 89
$3d\delta\ ^3\phi_4$	0.038 24	$4d\pi\ ^3\Sigma_1^+$	− 0.017 60
$3d\delta\ ^1\phi_3$	0.035 54	$4d\pi\ ^1\Sigma_0^+$	− 0.053 44
$3d\pi\ ^3\Delta_1$	0.009 67	$4s\sigma\ ^3\Pi_0$	1.1999(4)
$3d\pi\ ^3\Delta_2$	0.000 46	$4s\sigma\ ^3\Pi_1$	1.1978
$3d\pi\ ^3\Delta_3$	0.009 15	$4s\sigma\ ^3\Pi_2$	1.2005(4)
$3d\pi\ ^1\Delta_2$	− 0.02 081	$4s\sigma\ ^1\Pi_1$	1.1999
$4d\pi\ ^3\Delta_3$	− 0.003 58(1)	$5s\sigma\ ^3\Pi_0$	1.2078
$3d\pi\ ^1\Sigma_0^-$	0.019 29	$5s\sigma\ ^3\Pi_1$	1.2046
$3d\pi\ ^3\Sigma_1^-$	− 0.001 88(2)	$5s\sigma\ ^3\Pi_2$	1.2079
$3d\pi\ ^3\Sigma_0^-$	− 0.010 82	$5s\sigma\ ^1\Pi_1$	1.2056
$3d\pi\ ^3\Sigma_0^+$	0.002 58		
$3d\pi\ ^3\Sigma_1^+$	− 0.003 65		
$3d\pi\ ^1\Sigma_0^+$	− 0.041 98		

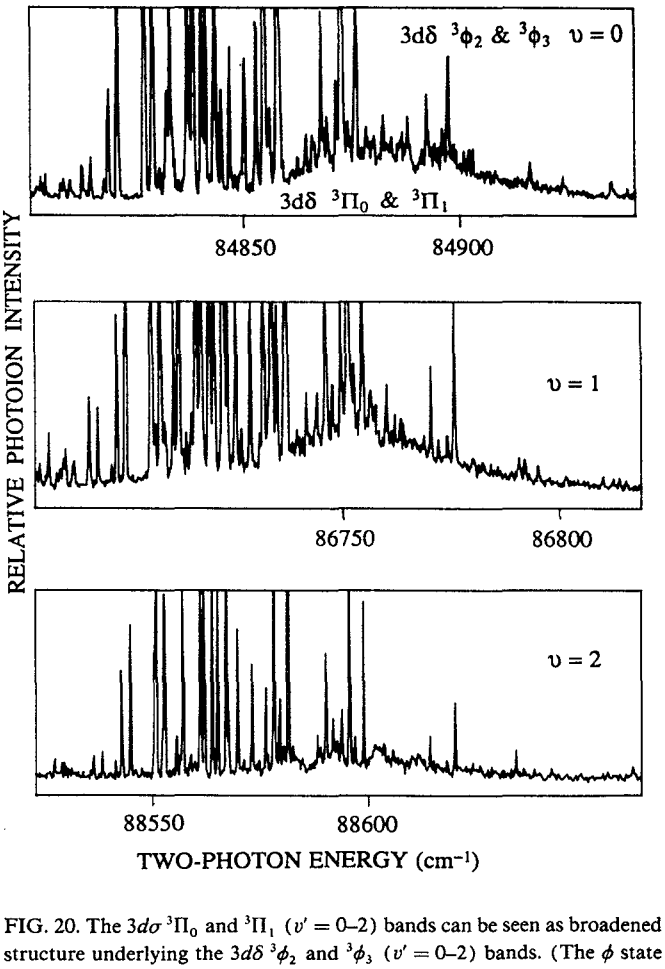

FIG. 20. The $3d\sigma\ ^3\Pi_0$ and $^3\Pi_1$ ($v' = 0$–2) bands can be seen as broadened structure underlying the $3d\delta\ ^3\phi_2$ and $^3\phi_3$ ($v' = 0$–2) bands. (The ϕ state peaks are assigned in Fig. 9 of Ref. 1.)

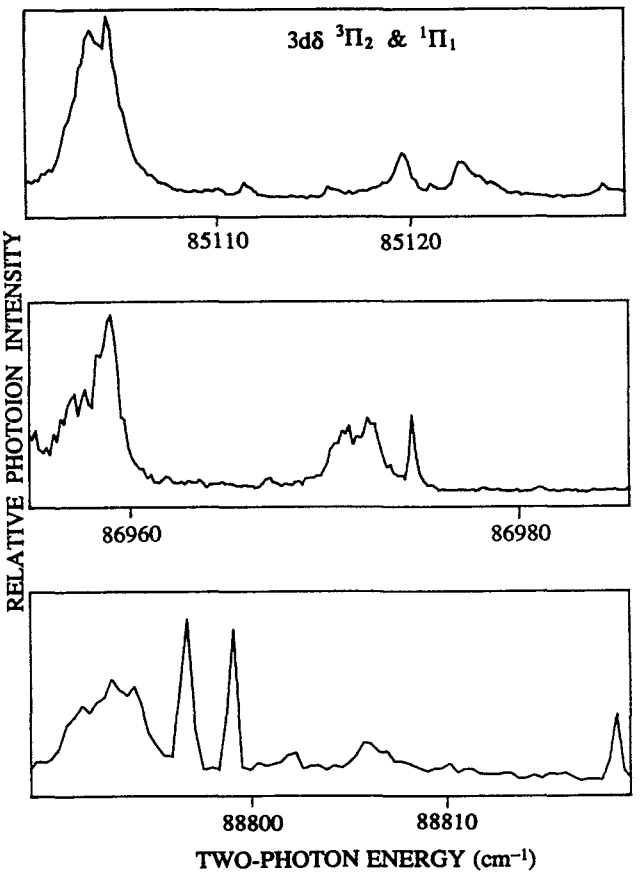

FIG. 21. The broad peaks thought to be due to the $v' = 0$–2 levels of the $3d\delta$ $^3\Pi_2$ and $^1\Pi_1$ states are shown. The sharp peaks were assigned to the $^3\Delta_1$ and $^3\Delta_2$ states in earlier work.

certain that they are located very close to the calculated location, as was the case for the other $3d\delta$ states, namely, the ϕ states.

M. The $3d\sigma$ Π states

In a search for $3d\sigma$ Rydberg states we have scanned up to 200 cm^{-1} above the observed $^1\Sigma_0^+$ band for $v' = 0$ and 1, and the complete interval between $v' = 2$, 3, and 4 with our highest laser power and observed no structure which could not be assigned to the states already discussed. We conclude that these states may be too weakly excited and overlapped by other bands to a point which precludes their detection, or they are too strongly homogeneously predissociated to be detected in our experiment.

N. Production and detection of oxygen atoms

While measuring the spectrum of the $v' = 1$ level of the $3d$ Rydberg states we detected sharp peaks in the O^+ channel which do not have counterparts in the O_2^+ channel. This is normally the signature of an atomic resonance in our experiments. Other explanations are possible though highly unlikely. The peaks we detect occur at 87 188.4, 87 191.9, and 87 196.2 cm^{-1} assuming they are 2 + 1 REMPI resonances. These peaks are so far unassigned, but it seems quite unlikely that they are due to O (^3P) atoms absorbing any combination of fundamental or doubled laser photons since an examination of tables of atomic energy levels yields no excited states at the appropriate energies. Another possibility is the resonant ionization of O (^1D) atoms. The $1\,^3\Pi_g$ repulsive valence state dissociates to two O (^3P) atoms in the adiabatic representation and to O (^3P) + O(^1D) in the diabatic representation. Predissociation by this state leads to production of both states of the atom and this branching ratio has been the subject of a recent investigation.[17] It would be interesting if the O^+ peaks we are detecting are indeed due to ionization of O (^1D) atoms as there would then be an MPI detection scheme at a very convenient wavelength for this metastable and highly reactive species. At present the only MPI detection scheme requires the use of photon wavelengths in the much less convenient wavelength region of about 202 nm. However, an examination of tables of the known energy levels of atomic oxygen does not lead to the identification of any resonant level which would explain the observed lines as due to resonant MPI of either the ^3P, ^1D, or ^1S levels of ground configuration oxygen atoms. We are forced to the conclusion that, either the lower state belongs to an excited configuration or the upper state is not included in the current tables, or both. The possibility of an unreported upper state being responsible for the resonance is not at all small since even current compilations report very many sharp lines belonging to states above the ionization limit and an examination of the relevant configurations indicates that many other similarly long-lived levels should exist.

Measurement of the photoelectron spectrum associated with these peaks should be able to establish their atomic origin as well as the number of photons producing the resonance. Production of oxygen atoms in other than the ground configuration would be very unexpected and could lead to better understanding of the photophysical behavior of O_2 in laser fields of moderate power.

IV. CONCLUSION

The present work has added the following information to that of previous studies:

(1) The pertubations in the rotational structure of the Σ states are better understood and the rotational assignments for many of the Σ states are presented.

(2) The $^1\Sigma_0^-$ state is definitively located for $v' = 0$–2.

(3) The $4s\sigma$ Π, $5s\sigma$ Π, and $3d\delta$ Π states have been located, their linewidths estimated for several values of v', and in some cases rotationally assigned. The $4s\sigma$ Π states are shown to be responsible for many of the pertubations in the $3d\pi$ Σ states. Other pertubations, in particular predissociation of the Σ states, are ascribed to the interaction with the $1\,^{1,3}\Pi_g$ repulsive valence states. The $ns\sigma$ Π states are shown to display expected trends in singlet–triplet splitting, linewidth, and intensity.

(4) The analysis for many $nd\lambda$ states has been extended to higher energies to include $3d\lambda$ $v' = 4$ and $4d\lambda$ $v' = 0$, and 1 states. As a result, the eigenvectors for the $nd\pi$ states can be given for $n = 3$ and 4 and can be extrapolated to higher values of n.

(5) The entire 2 + 1 REMPI spectrum of O_2 from 83 000 to 93 000 cm^{-1} has now been measured with independent wavelength calibration using the optogalvanic effect in a uranium hollow cathode lamp. Tables are given to present the energies of the origins of many of the 184 bands predicted to exist in the regions scanned.

Note added in proof. Current work indicates that the $ns\sigma\ ^1\Pi_1$ assignments should be considered tentative.

ACKNOWLEDGMENTS

The authors wish to thank Dr. Helene Lefebvre-Brion for many helpful discussions. This work was supported by the National Science Foundation (CHE-8821032).

[1] R. J. Yokelson, R. J. Lipert, and W. A. Chupka, J. Chem. Phys. **97**, 6144 (1992).
[2] H. Park, L. Li, W. A. Chupka, and H. Lefebvre-Brion, J. Chem. Phys. **92**, 5835 (1990).
[3] A. Recknagel, Z. Phys. **87**, 375 (1934).
[4] R. O. Loo, W. J. Marinelli, P. L. Houston, S. Arepalli, J. R. Wiesenfeld, and R. W. Field, J. Chem. Phys. **91**, 5185 (1989).
[5] H. Lefebvre-Brion and R. W. Field, *Pertubations in the Spectra of Diatomic Molecules* (Academic, Orlando, 1986).
[6] L. Sanche and G. J. Schulz, Phys. Rev. Lett. **26**, 943 (1971).
[7] D. C. Cartwright, W. J. Hunt, W. Williams, S. Trajmar, and W. A. Goddard III, Phys. Rev. A **8**, 2436 (1973).
[8] A. Sur, C. V. Ramana, and S. D. Colson, J. Chem. Phys. **83**, 904 (1985); A. Sur, C. V. Ramana, W. A. Chupka, and S. D. Colson, J. Chem. Phys. **84**, 69 (1986).
[9] R. D. Johnson III, G. R. Long, and J. W. Hudgens, J. Chem. Phys. **87**, 1977 (1987).
[10] R. S. Friedman and A. Dalgarno, J. Chem. Phys. **93**, 2370 (1990).
[11] R. S. Friedman, M. L. Du, and A. Dalgarno, J. Chem. Phys. **93**, 2375 (1990).
[12] H. Park, P. J. Miller, W. A. Chupka, and S. D. Colson, J. Chem. Phys. **89**, 6676 (1988); **89**, 3919 (1988).
[13] H. Park, L. Li, and W. A. Chupka, Chem. Phys. Lett. **162**, 317 (1989).
[14] H. Park, L. Li, and W. A. Chupka, J. Chem. Phys. **92**, 61 (1990).
[15] P. J. Miller, L. Li, W. A. Chupka, and S. D. Colson, J. Chem. Phys. **89**, 3921 (1988); J. A. Stephens, M. Braunstein, and V. McKoy, J. Chem. Phys. **89**, 3923 (1988).
[16] Ch. Jungen, J. Chem. Phys. **53**, 4168 (1970).
[17] J. P. Peterson and Y. K. Bae, Phys. Rev. A **30**, 2807 (1984); W. J. van der Zande, W. Koot, J. R. Peterson, and J. Los, Chem. Phys. Lett. **140**, 175 (1987); W. J. van der Zande, W. Koot, J. Los, and J. R. Peterson, J. Chem. Phys. **89**, 6758 (1988); W. J. van der Zande, W. Koot, J. R. Peterson, and J. Los, Chem. Phys. **126**, 169 (1988); W. J. van der Zande, W. Koot, and J. Los, J. Chem. Phys. **91**, 4597 (1989).